IEEE Access
Multidisciplinary | Rapid Review | Open Access Journal

Received June 3, 2021, accepted July 3, 2021, date of publication July 6, 2021, date of current version July 16, 2021.

Digital Object Identifier 10.1109/ACCESS.2021.3095105

IFFT-Based Microwave Non-Destructive Testing for Delamination Detection and Thickness Estimation

GHASSAN NIHAD JAWAD[1], (Member, IEEE), AND MUHAMMAD FIRDAUS AKBAR[2], (Member, IEEE)

[1]College of Engineering, University of Baghdad, Baghdad 10071, Iraq
[2]School of Electrical and Electronic Engineering, Universiti Sains Malaysia, Pulau Pinang 14300, Malaysia

Corresponding author: Muhammad Firdaus Akbar (firdaus.akbar@usm.my)

This work was supported by the Ministry of Education Malaysia Fundamental Research Grant Scheme (FRGS) under Grant 203.PELECT.6071430.

ABSTRACT Microwave Non-Destructive Testing (NDT) techniques for dielectric coatings are vital processes in many industrial applications due to their superior defect detection capabilities over traditional NDT methods. However, the limited bandwidth and post-processing complexities of these techniques cause them to fall short of accurately estimating the delamination thickness in such structures. In this paper, a novel low-complexity signal processing method is proposed to estimate the delamination thickness in metal-backed dielectric coatings using bandwidth-limited Open-Ended Rectangular Waveguide (OERW) probes. Here, Inverse Fast Fourier Transform (IFFT) process is used to convert the measured complex reflection coefficients at the surface of the coating to the time domain. Next, the amplitude of a specific time step is used to accurately estimate the delamination thickness without extra time-consuming processing. Using a 3 mm-thick macor samples with machined defects, the proposed technique is validated by correctly estimating delamination thickness down to 0.4 mm using an OERW probe with 13.5 GHz bandwidth. Hence, this technique overcomes the challenge of the OERW's limited bandwidth, which highly affects the possibility of tracking shifting in the peak reflection in the time domain. Moreover, the proposed method does not add to the complexity of the NDT process, which makes it suitable for in-situ real time applications. Hence, following this approach would be of great importance to numerous industries, where accurate thickness estimation of minute delamination in coatings is essential to avoid system failure.

INDEX TERMS Microwave NDT, TBC delamination, thickness estimation, IFFT.

I. INTRODUCTION

Polymer composites are widely used in many industries such as construction, power plants, and aerospace. For instance, applying ceramic based Thermal Barrier Coatings (TBCs) onto metal surfaces of gas turbine components maintains their durability as the surrounding temperature increases [1]. However, various factors, such as thermal stress and expansion mismatch, can cause delaminated areas to appear between the TBCs and the substrate of the component, as shown in Figure (1) [2]. The existence of such areas could cause major failures if not immediately repaired [3]. Moreover, to avoid catastrophic consequences, early detection of delaminated regions in vital system parts is imperative. Hence, it is important for any Non-Destructive Testing (NDT) technique to be able to detect such material failures in the early stage, which means being able to identify areas with the lowest possible delamination thickness.

Generally speaking, numerous non-destructive Testing (NDT) methods are being used to detect such defects [4]–[7]. However, despite their success in detecting defects in metals, most of these approaches fail to detect delaminated regions with small thickness inside polymer composite materials.

Alternatively, other techniques have been reported to specifically inspect TBC delamination. Two principal technologies are used for this purpose, namely Infra-Red Thermography (IRT), and THz technology. IRT relies on heating

The associate editor coordinating the review of this manuscript and approving it for publication was Xiaokang Yin.

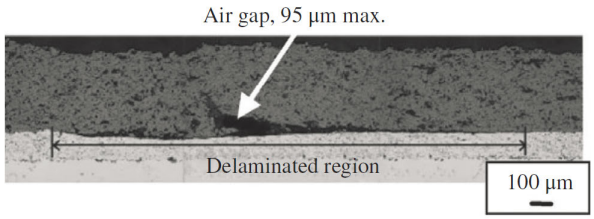

FIGURE 1. Cross section of delaminated region of a thermal barrier coating (TBC) sample [2].

the TBC sample using a heat source (usually a laser or a flash lamp), and record the change in the temperatures in different parts of the sample using an infra-red detector (or camera) [2], [8]–[15]. Despite the ability of this technique to detect and estimate the thickness of shallow delaminated areas in TBC samples, reliable and accurate results rely on increasing the complexity of the setup and the post-processing steps. Therefore, in practice, inspecting TBCs for delamination represents a significant challenge. On the other hand, THz technology is based on electromagnetic interactions between the TBC layer and signals in the THz frequency range (usually $0.1 - 10$ THz) [16], [17]. THz inspection is conducted by transmitting a short pulse into the sample and inspect its reflections from the various discontinuities inside the material. Therefore, the depth resolution provided by this method relies solely on the bandwidth of the incident signal, which is usually set to few-hundreds GHz. The generation of such signal is usually done using a femotosecond laser that initiates the pulse from a transmitting antenna [16]. Therefore, this NDT technique mandates a costly apparatus to obtain an accurate estimation of delamination thicknesses.

Because of the above, alternative microwave-based NDT techniques have emerged [18]–[23]. The main advantage of these techniques is the ability of electromagnetic signals in the microwave frequency range to penetrate dielectric coatings. In addition, unlike THz pulses, generating microwave signals can be done using modern solid-state based circuits and components. Therefore, microwave reflections from the TBC internal structure could be collected and processed using relatively simple and low-cost setups. Most of microwave NDT approaches depend on scanning the surface of the dielectric with an Open-Ended Rectangular Wavegiude (OERW) probe, and record the reflections at discrete frequency points. Consequently, frequency domain reflections could be mathematically processed to reveal the accurate dielectric thickness [24], [25]. Despite their accuracy, such methods suffer from computational complexity, which limits their usage in real-time NDT applications.

Recently, an alternative microwave NDT approach has been proposed to reveal small changes in various type of dielectric coating by converting the recorded reflections to the time domain. By doing so, the reflections from various discontinuities inside the dielectric were detected by tracking the reflected pulses to the OERW probe [21], [23]. Such methods are similar to the well-established Time Domain Reflectometry (TDR) method used to estimate the defects' locations in faulty cables [26], and also the previously mentioned THz technology [16], [17]. However, the main drawback of time domain microwave NDT techniques is that, contrary to the TDR and THz technologies, they use bandwidth-limited OERW as a probe. This limitation highly affects the resolution of the detection, which is inversely proportional to the bandwidth of microwave signal used for detection. To overcome this limitation, a modified TDR method is proposed in [27] to track the amplitude of the peak in the measured time domain reflection peak instead of tracking the time shift of the peak itself. Despite the ability of this method to detect various defects, estimating the delamination thickness proved to be challenging due to the nonlinear relation between the reflection peak amplitude and the actual time shift. Another method proposed in [23] used zero-padding on the measured frequency domain reflection coefficient in order to artificially increase the bandwidth of the signal. This process has the effect of oversampling the time domain signal, which causes the reflection pulses to be more pronounced and hence, provides the possibility of tracking the shift in the peak reflection in the time domain. However, this method increases the computational complexity of the NDT process because of the increased data points, which limits its applicability in real-time NDT applications.

In this paper, a novel low-complexity microwave NDT method is proposed for delamination detection and thickness estimation. In this method, the Inverse Fast Fourier Transform (IFFT) algorithm is used to convert the measured frequency domain reflection coefficient to the time domain. Next, based on a reference measurement, a certain time step is identified to tack its amplitude for all the scanned locations. The variation in the reflection amplitude is then normalized and compensated for the nonlinearity using a pre-defined sinc function to reveal an accurate estimation of the distance to the source of reflection (in this case, the location of the delaminnation). Relying on the amplitude variations of IFFT results to obtain the delamination depth information represents a significant advantage over tracking the shift of the reflected peaks, as in the THz technology [16], [17] and previously-reported microwave NDT techniques [23]. This is due to the simplicity, narrow bandwidth, and low cost of the NDT setup when compared to the one used in the THz technology. In addition, obtaining the time domain data using the efficient IFFT algorithm without the need to zero-pad the frequency domain measurements reduces the duration of the post-processing steps, which makes the proposed technique more suitable for real-time applications.

The rest of this paper is organized as follows: section II gives an overview of the basic theoretical background necessary for understanding the proposed technique. In section III, the proposed technique is outlined in details, followed by applying the technique to two arrangements to evaluate its capabilities. Processing the measured data for two samples using the proposed techniques is described and discussed in Section IV. Finally, Section V provides the main conclusions

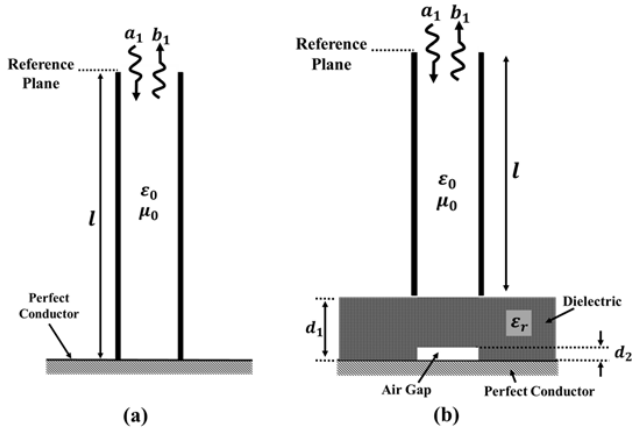

FIGURE 2. Open-ended waveguide structures considered for analysis: (a) OERW terminated with a perfect conductor, and (b) OERW terminated with a metal-backed sample with delamination.

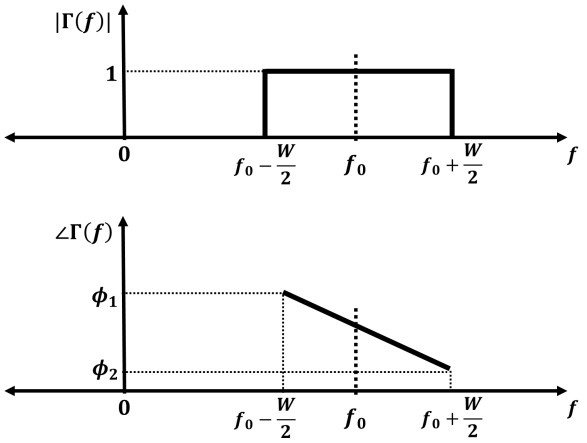

FIGURE 3. Magnitude and phase of the reflection coefficient for the waveguide arrangement shown in figure (2-a).

drawn from the analysis and results outlined in the previous sections.

II. THEORETICAL BACKGROUND

Basic microwave network theory dictates that an OERW probe can be regarded as a one-port network, where the reflection coefficient at the input is defined as follows [28]:

$$\Gamma(f) = \frac{b_1(f)}{a_1(f)} \tag{1}$$

where a_1 and b_1 are the frequency-dependent normalized incident and reflected power waves at port 1, respectively.

The principles of Time Domain Reflectometry (TDR) is based on detecting the arrival time of a pulse sent from the probe towards the source of reflection. Based on the recorded time of arrival of the pulse, the distance towards the source of reflection can be deduced [29]. To apply this method, it is imperative for the pulse to have ultra-short rise time to allow distinguishing between adjacent sources of reflection. Consequently, the signal needs to have an extra wide bandwidth to cope with such requirement. On the other hand, a rectangular waveguide can only be operated within the dominant TE_{10} mode, which depends on the dimensions of the waveguide's cross-section [30]. This will result in a relatively wide pulses in the time domain, which renders applying classical TDR techniques using OERW impractical.

Here, a basic theoretical analysis is outlined for two OERW arrangements: the first is a simple l-long rectangular waveguide shorted at the end, as shown in Figure (2-a). The second structure, on the other hand, is an OERW of the same length, but with its open-end directly placed on a d_1-thick dielectric layer backed by a conductor. To account for the existence of a delamination, an air-pocket of thickness (d_2) is considered to exist within the dielectric layer directly above the conductor, as shown in Figure (2-b).

It is worthwhile to mention that the input port to the waveguide is assumed to be well matched to the measurement system such that multiple reflections can be ignored.

A. SHORTED RECTANGULAR WAVEGUIDE

For the arrangement shown in Figure (2-a), given the limited range of frequencies for this waveguide, the magnitude of the complex reflection coefficient can be expressed as a rectangular pulse in the frequency domain:

$$\Gamma(f) = A\ rect\left(\frac{f - f_0}{W}\right) e^{j\phi(f)} \tag{2}$$

where $rect(.)$ is the rectangular function, f_0 is the central operating frequency of the waveguide, and W is the bandwidth of the operation. By neglecting the conductor loss in the OERW and the reflecting plate at the open end, the magnitude of the reflection coefficient (A) is considered to be unity for all the frequencies. However, the phase will be directly related to the length of the waveguide (l), in addition to the frequency-dependent phase constant ($\beta(f)$).

As shown in (3), the phase of the reflection coefficient is a function of f, and it can be described as follows:

$$\phi(f) = 2\beta(f)l \tag{3}$$

However, as a non-TEM media, rectangular waveguides feature a phase constant (β) that is, in general, a nonlinear function of the frequency. However, the frequency band of operation can be carefully chosen to ensure a region where $\beta(f)$ is a linear function. Hence, a linear phase can be assumed within the frequency range of interest, as shown in Figure (3).

Using basic Fourier analysis, the magnitude of the frequency domain reflection coefficient in (1) can be expressed in the time domain as [30]:

$$|\Gamma(t)| = 2A\,\pi W\ sinc\left(\pi W(t - \frac{2l}{v_g})\right) \tag{4}$$

where $v_g = \left(\frac{d\beta(\omega)}{d\omega}\right)^{-1}$ is the group velocity of the wave inside the rectangular waveguide. When a linear relationship between phase constant and frequency is maintained, the resulted group velocity will be constant within the frequency range of interest [30].

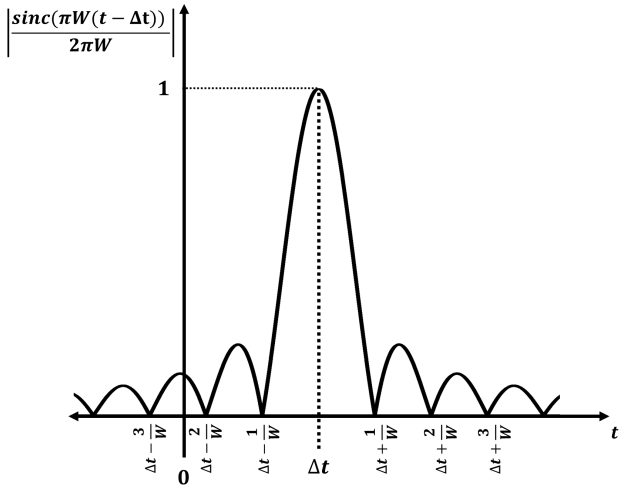

FIGURE 4. Magnitude of the reflection coefficient in the time domain shifted by Δt.

It can be seen from (4) that the sinc function is shifted in the time domain by ($\Delta t = \frac{2l}{v_g}$), which is the time required for the pulse to reach the reflector at the end of the waveguide and travel back to the reference plane. A normalized reflection pulse shifted by Δt is plotted in Figure (4). Given that the frequency domain data is, in practice, provided at N discrete frequency points over the bandwidth of operation. These points can be efficiently converted to the time domain by applying the Inverse Discrete Fourier Transform (IDFT). Usually, IDFT is efficiently calculated using the Inverse Fast Fourier Transform (IFFT) algorithm. Using the IFFT on the N-points frequency domain data, the result will also be N-points discrete time domain data separated by $1/W$ seconds and span for N/W seconds.

Given the reflection coefficient at discrete frequencies ($\Gamma(nf), n = 0, 1, 2, .., N$), the resulted time domain function ($|\Gamma(k)|, k = 0, 1, 2, .., N$) can be viewed as a sampled version of the sinc function in (4) with a time spacing of ($T = 1/W$).

According to the principles of TDR, detecting the shift in the peak of $|\Gamma(t)|$ would provide information about the unknown distant to the source of reflection (in this case, the length of the waveguide, l). However, for bandwidth-limited measurements, the shift in the peak of the sampled version of the time domain data will not be apparent for time shifts of less than $1/W$ seconds. This will cast a serious hindrance towards the ability of frequency-limited measurement probes, such as OERW, to detect minute changes in the reflection distance.

It is worth noting that finding the IFFT with higher number of points can provide better depiction of the reflected pulse since it operates oversampling in the time domain (or zero-padding in the frequency domain) [23]. However, that would highly increase the computational complexity of the detection technique and compromise the ability of the NDT system to track the shift in the peak of the resulted sinc function in the real time. However, by analyzing the relationship between the sinc function in (4) and the sampled version resulted from applying IFFT to the $N-$points frequency domain reflection coefficient, it can be seen that there is a relation between the *amplitude* at certain time steps in the IFFT data and the actual shift in the sinc function. This would allow detecting the smallest change in Δt even when the bandwidth of the measurement (W) is limited.

Figure (5) shows the reflection coefficient magnitude in the time domain for two time shifts, namely Δt_1 and Δt_2. On the same graphs, the first seven steps of the sequence that would be obtained using IFFT are marked. It can be noticed from Figure (5-a) that the peak of the IFFT occurs at $k = 2$, which is associated with $t = 2/W$ seconds with a peak magnitude of P_1. When the time of arrival (Δt) shifts down by a small amount (less than $1/W$), the peak remains at $k = 2$. However, the magnitude of the peak increases to P_2. Hence, despite the inability of the traditional TDR method to detect the existence (and the amount) of time shift, it is possible to detect the shift by observing the magnitude of the IFFT data peak. Additionally, the amount of the shift in the time ($\Delta t_1 - \Delta t_2$) can also be estimated to a reasonable degree of accuracy.

From above, it can be concluded that it is possible to track the changes in the length of the waveguide in the arrangement shown in Figure (2-a) by tracking the amplitude changes of the N-points time domain reflection coefficient resulted from IFFT. However, to provide accurate estimation for the amount of change in the length, the increase (or decrease) in the amplitude of the IFFT results has to be mapped to actual lengths. Nevertheless, it can be deduce from (4) that the relation between the reflection coefficient in the time domain ($|\Gamma(k)|$) and the time shift (Δt) is nonlinear. Hence, there is a need to apply an algorithm to inverse the sinc function in (4) to account for the nonlinearity in the estimation.

B. MULTIPLE REFLECTIONS

To consider the multiple reflections scenario that accounts for the realistic delamination detection NDT scanning, the arrangement shown Figure (2-b) is analyzed next. In this arrangement, the waveguide's open end is placed on the surface of a d_1-thick dielectric layer backed by a metal. The dielectric layer contains an air gap (that resembles a delamination) with a thickness of d_2 directly below the waveguide's aperture.

Compared to the shorted waveguide structure in Figure (2-a), the reflections from this arrangement are affected by numerous factors, the most important of which are the multiple reflections inside the dielectric and the excitation of higher-order modes near the waveguide's open end. These factors might highly affect the detection and thickness estimation process when the dielectric thickness is high compared to the wavelength of operation. In practice, however, the dielectric thickness for dielectric coatings doesn't exceed few millimeters, and the delamination thickness doesn't usually exceed a fraction of that. Hence, an assumption can be

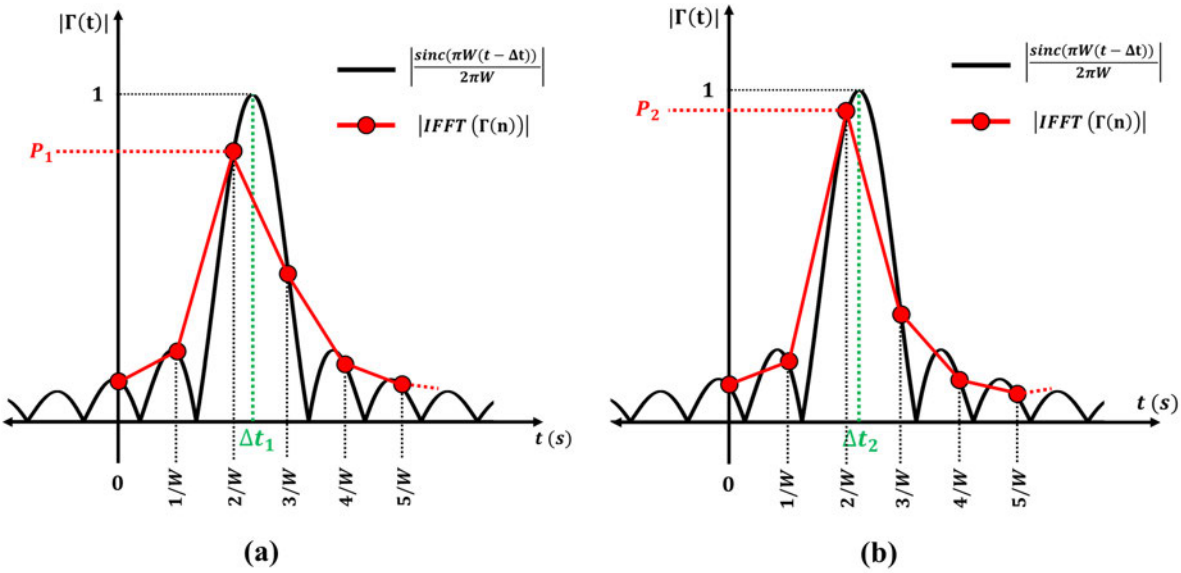

FIGURE 5. Effect of shift on the time domain magnitude of the reflection coefficient resulted from a single-reflection arrangement with time shift of (a) Δt_1, and (b) Δt_2.

made to ignore the multiple reflections inside the dielectric and the waveguide maintains the dominant TE_{10} mode in the vicinity of the probe's open end.

From Figure (2-b), it can be seen that the expected number of reflections is three: the first one originates from the interface between the open-ended waveguide and the surface of the dielectric. The second reflection comes from the interface between the dielectric and the air gap, and the interface at the back metal represents the third and final reflection. Hence, the complex reflection coefficient in the frequency domain can be expressed as [31]:

$$\Gamma(f) = rect\left(\frac{f - f_0}{W}\right)\left[Ae^{j\phi_1(f)} + Be^{j\phi_2(f)} + Ce^{j\phi_3(f)}\right] \quad (5)$$

Here, the reflection amplitudes A, B, and C depend on the relative permittivity of the dielectric layer. The phase shifts, on the other hand, are defined as follows: $\phi_1(f) = 2\beta(f)l$, $\phi_2(f) = 2\beta(f)(l + d_1 - d_2)$, and $\phi_3(f) = 2\beta(f)(l + d_2)$.

Applying the inverse Fourier transform to (5) will result in the following time domain reflection coefficient magnitude:

$$|\Gamma(t)| = 2\pi W\left[A\ sinc\left(\pi W(t - \frac{2l}{v_g})\right) + B\ sinc\left(\pi W(t - \frac{2(l + d_1 - d_2)}{v_g})\right) + C\ sinc\left(\pi W(t - \frac{2(l + d_1)}{v_g})\right)\right] \quad (6)$$

The addition of the three terms of (6) will cause the sinc functions to mix, especially the second and third terms when d_2 is in the order of a fraction of a millimeter. However, for a delamination-free region, the second term in (6) will vanish since the reflection from the dielectric/delamination interface does not exist. Therefore it is expected for the time domain reflection coefficient to feature two peaks; one for the waveguide/dielectric interface, and another one from the back metal. However, when a small delmaination exists between the dielectric and the back metal, the second peak will be changed due to the existence of a new reflection that merges with it and shifts it down in time as the delmaination thickness (d_2) gets larger.

To detect a delamination, it is necessary to track the magnitude of one of the IFFT time steps that is related to the second peak for a reference reading. This reference reading it taken to be at a previously known delamination-free location. From this reading in the frequency domain, it is required to find the actual shape of the pulses in order to determine the exact location for the IFFT time step to be tested for the rest of the scan. To do this, the oversampling implemented in [23] will be implemented on the reference reading so that the result will resemble the reflection waveform shown in Figure (6). After obtaining these results, the time step at which the second peak appears will be noted and the associated time step in the IFFT results will also be known. Consequently, as the reflection peak shifts down in time, the amplitude of this time step will increase, and it will decrease if the shift goes the other way.

To obtain the accurate the shift in the time, the sinc function has to be inverted to reveal the time shift associated with the increase/decrease in the normalized amplitude of the considered IFFT time step. Figure (6) shows the magnitude of the time domain reflection coefficient obtained using (6), assuming equal magnitude for all the reflections (A, B, and C). Here, two cases for the second reflection are considered, namely Δt_1 and Δt_2, where $\Delta t_1 < \Delta t_2$. On the same graph, the sequence of $\Gamma(k)$ that would be obtained when applying IFFT to the frequency domain data have also been plotted. It can be noticed that the second peak of the reflection

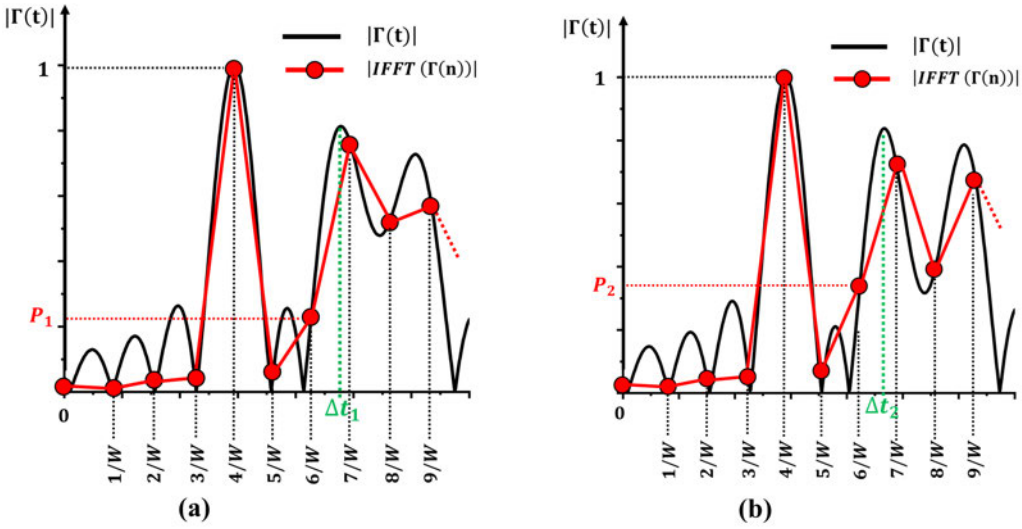

FIGURE 6. Effect of shift on the time domain magnitude of the reflection coefficient resulted from a multiple-reflection arrangement with times shift of (a) Δt_1, and (b) Δt_2.

magnitude in the IFFT shows a decrease when the reflection time shifts from Δt_1 in Figure (6-a) to Δt_2 in Figure (6-b). It can also been seen that no significant change can be noticed on the amplitude of the first reflection.

It can be concluded from above that it is possible to detect delamination areas and estimate their thickness by tracking the amplitude of the IFFT-based time domain reflection coefficient at a fixed time step. However, finding the correct time step and the reduction/increase in the magnitude would require additional steps to be performed by the detection/estimation algorithm, as will be illustrated in the next section.

III. PROPOSED TECHNIQUE

The proposed technique aims to work on the arrangement shown in Figure (2-b) to detect and estimate the thickness of delamination areas between the dielectric coating and the back metal. The technique uses an OERW probe to scan the surface of the dielectric while recording the reflection coefficient (as S_{11}) at N discrete frequency points. For each scanned location, N-points IFFT is applied to obtain the time domain equivalent of the reflection coefficient, namely $|\Gamma(k)|$.

The detection and estimation algorithm can be outlined as follows:

1) N-points frequency domain *reference* reflection coefficient ($|\Gamma_r(n)|$) data are recorded for a previously-identified delamination-free location.
2) The recorded reference reflection coefficient is processed by applying M-points IFFT to get the time domain reference reflection coefficient $|\Gamma_r(k)|$, where $M \gg N$. The resulted data represents the over-sampled version of the N-points IFFT, and will be used to identify the locations of the peaks in the time domain reflection coefficient. Calculating the M-points IFFT might consume more time than other processes in the algorithm, but it does not add to the overall complexity of the technique since it is only calculated once.
3) Using the previously known values of the waveguide length (l) and dielectric thickness d_1, the time shift associated with the location of the reflection peak (Δt_r) is found. Consequently, the estimated group velocity (v_{ge}) can also be found. Here, the chosen peak depends on the considered structure; for example, for the shorted waveguide shown in Figure (2-a), there is only one peak to be chosen. However, for the arrangement shown in Figure (2-b), the second peak is identified since it is the one that shifts with increased delamination thickness.
4) Using the recorded data, the time step for the M-points IFFT data (x_M) is found. This time step is used to find the time step to be tracked for the N-points time domain reflection coefficient, x_N using:

$$x_N = x_M \frac{N}{M} \tag{7}$$

For the rest of the sample, the magnitude of the N-points IFFT at x_N will be tracked and recorded.
5) Next, the scanning of the sample is started by moving the location of the OERW by a pre-defined steps and finding the frequency domain reflection coefficient at each location.
6) For each recorded reflection coefficient, N-points IFFT is applied and the value of $|\Gamma(x_N)|$ is recorded and normalized to the maximum amplitude obtained from the reference time domain reflection, $|\Gamma_r(k)|$.
7) The deviation from the reference time shift (Δt) is found for each location by mapping the changes in $|\Gamma(x_N)|$ for those locations on a reference sinc function.

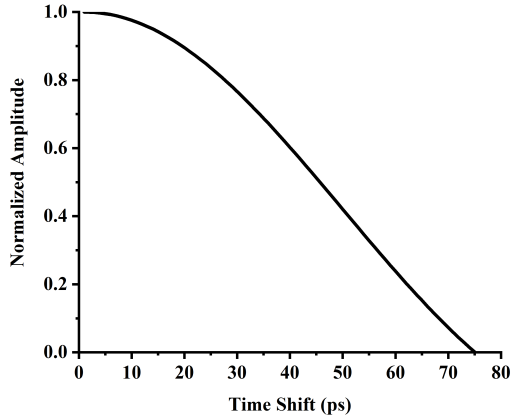

FIGURE 7. The sinc function used for the inverse time table time shift estimation (considering $W = 13.5$ GHz.)

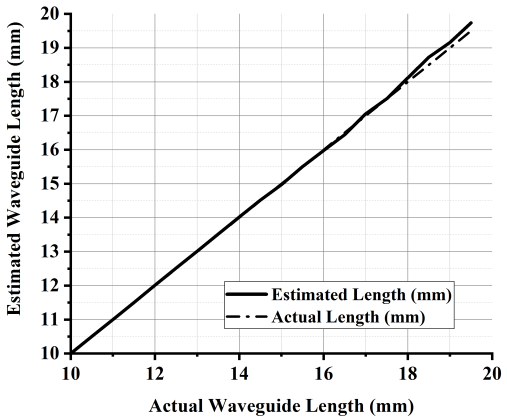

FIGURE 8. Estimated shorted waveguide length resulted from simulating the arrangement shown in figure (2-a).

This step is performed to account for the nonlinear nature of the amplitude changes by associating each value of the normalized amplitude to a certain time shift that is obtained from the function:

$$S = sinc(2\pi tW) \tag{8}$$

Figure (7) shows the sinc compensation function for $W = 13.5$ GHz. To apply this step, a look-up table is used to identify the time shift associated with each normalized amplitude.

From the above steps, the time shift associated with the reflection from the delamintion can be tracked. Using the previously calculated group velocity (v_{gr}), the distance to the source of reflection is found. Since the slightest shift in the reflection time can be detected, it is possible to detect shallow delamination areas and estimate their thickness.

To validate the proposed technique, the two arrangements shown in Figure (2) were simulated using the full-wave electromagnetic simulation package (CST MWS).

Starting with the shorted waveguide shown in Figure (2-a), a simulation model was created such that the waveguide length is increased from 10 to 20 mm with a step of 0.2 mm. By simulating the structure in the frequency domain, the reflection coefficient was recorded as S_{11}, and processed for each step as illustrated above.

Figure (8) shows the estimated waveguide length versus the actual length resulted from applying the proposed algorithm. It is clear that the proposed technique succeeds in estimating the waveguide length. This accuracy is due to the single-mode propagation nature of the waveguide structure, in addition to the lack of any source of loss in the waveguide or the reflector.

Next, the arrangement shown in Figure (2-b) was considered. Here, the OERW length (l) and the dielectric thickness (d_1) were assumed to be 10 mm and 3 mm, respectively. The dielectric layer was considered to be lossless with $\varepsilon_r = 5.2$. Here, the thickness of the delamination region between the dielectric and the back metal (d_2) is increased from 0 mm to 2.6 mm, with a 0.1 mm step. Applying the proposed technique to the simulated frequency domain reflection coefficients for each step resulted in the delamination estimation shown in Figure (9). The estimated delamination thickness for this arrangement has a margin of error of about 0.1 mm due to the assumptions applied in the estimation technique. However, there is a steady linear change of the estimated thickness with the actual thickness change of the delamination.

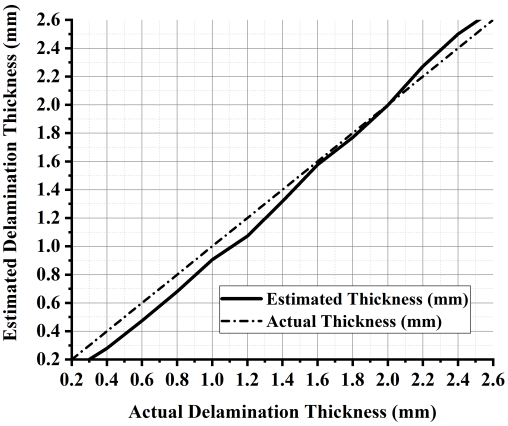

FIGURE 9. Estimated delamination thickness resulted from simulating the arrangement shown in figure (2-b).

The correct estimation of the thickness in the case of simulation results proves the validity of the technique to estimate delamination thickness with small margin of error, which qualifies it for reflection measurements on practical samples, as illustrated in the next section.

IV. RESULTS AND DISCUSSION

To perform practical validation for the proposed technique, two samples were fabricated using low loss glass ceramic (macor) with a dielectric constant of 5.67 at 8.5 GHz [23]. Both samples contained machined recesses with different areas and depths, as shown in Figures (10) and (11). To conduct the tests, the samples were pressed

against a metallic surface such that the machined recesses acted as differently-sized delamination regions, while scanning was performed on the upper (smooth) surface of the samples.

One-port reflection measurements were collected using a portable Vector Network Analyzer (VNA), calibrated to the end of a 2.92 mm coaxial wire. A WR-28 coaxial-to-waveguide adapter was used as an OERW probe to scan the surface of each sample. Recommended frequency band for the WR-28 was used by measuring the one-port scattering parameter (S_{11}) at 101 equally-spaced discrete frequency points from 26.5 to 40 GHz ($W = 13.5$ GHz) for each scanned location. For this VNA, the sweeping time required to obtain the reflection data for each scanned location is 432 μs. This time can be reduced by changing the Intermediate Frequency (IF) setting of the device [32]. Both scanning time and size of the apparatus could be further reduced by using a commercial one-port reflectometer analyzer, which is capable of performing the same task more efficiently [33]. It is worthwhile to notify that this experimental setup is very similar to numerous commercial NDT systems. Therefore, vital modules such as probe positioning system and processing unit used for other techniques, such as ultrasonic testing, can also be utilized for this technique with minimal modifications.

Figure (12) shows the experimental setup, where an automatic mechanical positioner was used to move the probe along the sample under test with pre-defined steps, while the VNA recorded the frequency domain reflection coefficient at each step.

The sample in Figure (10) was tested first. This sample contained five delamination areas with different sizes and depths. The OERW probe was placed on the surface of the sample (standoff distance = 0 mm), and oriented as illustrated in Figure (10-a).

After recording the reference reflection coefficient at a delamination-free location ($|\Gamma_r(n)|$), the inspection process started by scanning along the two lines highlighted in Figure (10-a) with 1 mm step.

Before performing IFFT on the scanned points, M-points IFFT was taken for the reference reflection coefficient. Here, M was set to 2^{14}, which artificially extends the bandwidth to 2211.7 GHz. This process revealed two distinct peaks; one for each source of reflection. As illustrated before, the time step for which the amplitude is to be tracked (x_N) was determined from the second peak, since it is the one affected by the existence of a delamination.

For each scanned location, after finding the 101-points IFFT, the normalized amplitude of $\Gamma(x_N)$ was found and converted to the associated time shift according to the pre-defined sinc function shown in Figure (7). Finally, the time shifts were converted to the estimated delamination thickness using the estimated group velocity found from the reference reading.

Figures (13) and (14) show the estimated delamination thickness resulted from scanning the first and second lines marked in Figure (10-a), respectively. It is clear from the

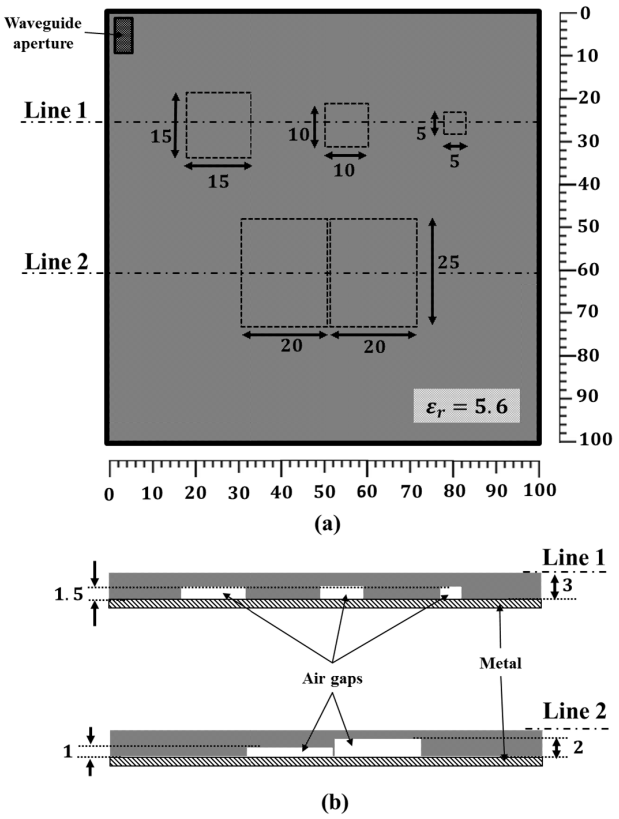

FIGURE 10. Layout of the first tested macor sample (a) top view, showing the locations of the delamination areas, (b) side view across the dashed lines marked in (a) (all dimensions are in mm, and the layouts are not drawn to scale).

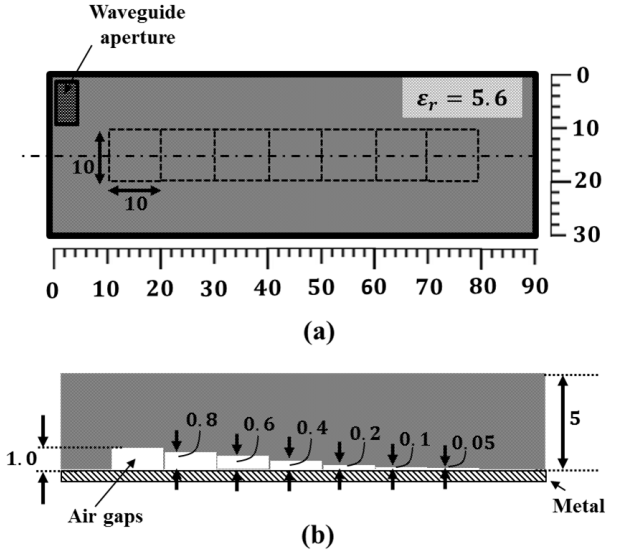

FIGURE 11. Layout of the second tested macor sample (a) top view, showing the locations of the delamination areas, (b) side view across the dashed line marked in (a) (all dimensions are in mm, and the layouts are not drawn to scale).

results that the proposed technique provides good estimation for the delamination areas in Line 1, where all three locations were identified correctly. However, it can be seen that

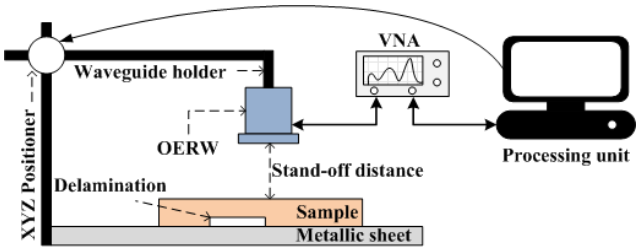

FIGURE 12. Diagram of the experimental setup.

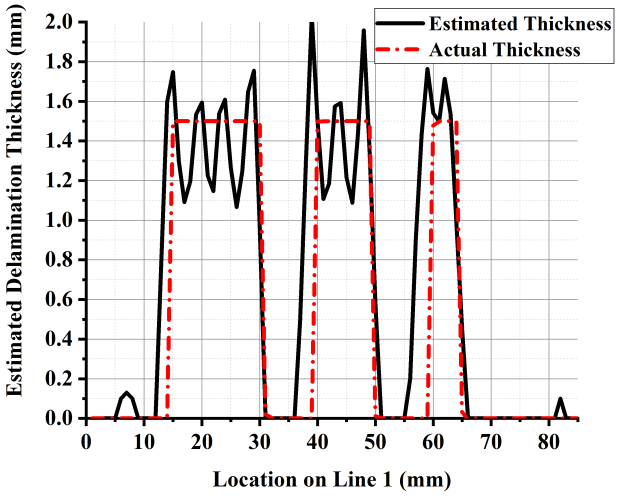

FIGURE 13. Estimated delamination thickness resulted from scanning along line 1 of sample 1.

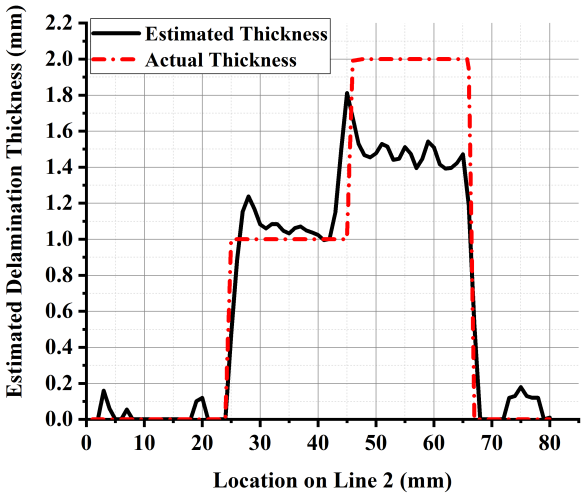

FIGURE 14. Estimated delamination thickness resulted from scanning along line 2 of sample 1.

the estimated thickness fluctuates around the mean value of 1.5 mm, which is the actual delamination thickness. These variations are attributed to the aperture effects of the OERW, where the distribution of the electric field would cause peaks in reflection when encounters sharp delamination edges. This problem can be compensated either by applying an averaging

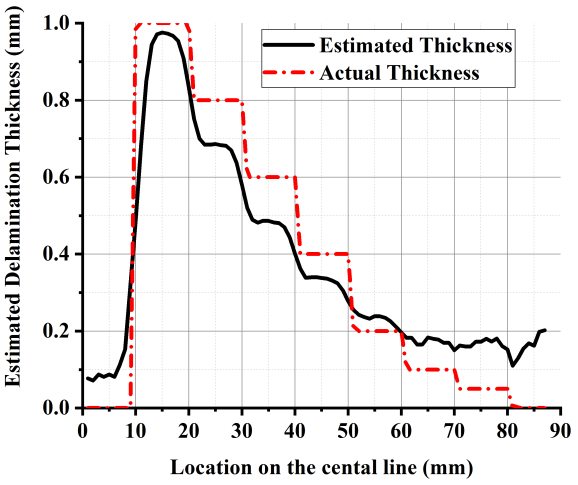

FIGURE 15. Estimated delamination thickness resulted from scanning along the central line of sample 2.

filter to the final estimation data [27], or by applying a de-convolution post processing steps to reverse the aperture effects of the OERW.

On the other hand, the estimated delamination thickness obtained from scanning Line 2 results in a close estimation for the 1 mm-thick delamination. However, the estimated thickness for the second delamination (2 mm-thick) shows an estimation error of about 0.5 mm. The inability of the technique to accurately estimate the thickness of the second delamination is due to the relatively large time shift of the second peak of the time domain reflection when encountering this delamination. This shift causes the peak of the pulse to pass the time step at which the amplitude is recorded and hence, results in an estimation error.

From above, it can be concluded that the proposed technique might show errors in estimating the thickness of delamination over a certain thickness. However, this can be corrected by adding another step to the aforementioned procedure to update the chosen time step (x_N) whenever the time shift passes a certain value. Nevertheless, since having delmaination with large thickness is unlikely, it is more important to focus on delamination areas with finer thickness, as in the second sample illustrated in Figure (11). This sample contains 7 machined delamination regions of equal areas (100 mm^2) with thickness varying from 1 mm to 0.05 mm. By scanning this sample along the line marked on Figure (11-a) and applying the same aforementioned processing steps, the estimated thickness shown in Figure (15) is obtained.

It can be seen form these results that the smooth depth changes in the delamination areas causes less fluctuations in the estimated thickness values. In addition, it is clear that the proposed technique is able to distinguish between the various sub-mm delmaination areas down to 0.2 mm. However, there is an error margin or about 0.1 mm for the delamination with thickness between 0.8 mm and 0.4 mm. Moreover, the

TABLE 1. A comparison between different microwave NDT techniques in terms of accuracy and complexity.

Reference	Proposal	Methodology	Accuracy (in thickness estimation)	Complexity
[18]	Dielectric thickness estimation	Phase measurement-based Microwave NDT	**Low**: the technique did not achieve an accurate phase-difference estimation when using OERW, therefore it was replaced by a horn antenna at higher frequency range ($75-110$ GHz)	**Low**: the technique is based on direct frequency-domain measurements. However, no further processing has been done to match the phase shift to the actual thickness estimation.
[22]	Dielectric thickness estimation	Principle component analysis-based Microwave NDT	**High**: The technique succeeded in estimating the thickness of dielectric coatings of pipes using a limited-bandwidth OERW arrangement	**High**: The technique requires applying Synthetic Aperture Radar (SAR) tomography to ensure feature extraction.
[35]	Dielectric thickness estimation	Genetic optimization algorithm-based Microwave NDT	**High**: The technique was able to provide accurate dielectric thickness estimation (within few-millimeter range) using X-band OERW	**High**: An iterative optimization method is required to minimize the cost function resulted from calculated and measured reflections.
[36]	Defect detection	Smooth nonnegative matrix factorization-based Microwave NDT	**Low**: The technique did not provide estimation for the thickness of the defects embedded in the dielectrics	**High**: Requires the application of Non-negative Matrix Factorization (NMF) algorithm in addition to smoothness constrains to extract the features of the sample.
[37]	Delamination detection	Bi-long short term memory-based Microwave NDT	**Low**:The technique showed the ability to detect shallow delamination *without* providing thickness estimation	**High**: The technique requires maximal overlap hybrid discrete wavelet packet transform for each frequency point.
[38]	Dielectric defects detection	Sum-average magnitude-based Microwave NDT	**Low**:The technique did not provide estimation for the thickness of the defects embedded in the dielectrics	**Low**:The technique processes the frequency domain data and applies filtering to reduce the effects of noise.
[39]	Dielectric defects detection	Circular probe phase response-based Microwave NDT	**Low**:The technique did not provide estimation for the thickness of the defects embedded in the dielectrics	**Low**:The technique is based on detecting the variation in the phase response of the reflected signal from an open-ended waveguide probe.
[40]	Dielectric defects detection	Artificial neural network-based Microwave NDT	**High**: The technique succeeded in detecting ring-shaped defects of small size without giving information about their thickness	**High**: Artificial Neural Networks (ANN) algorithms have to be used to preform the detection.
[41]	Delamination detection	K-means clustering algorithm-based Microwave NDT	**Low**: The technique showed the ability to detect shallow delamination without thickness estimation	**High**: Extensive post- and pre-processing is required for the technique to perform the detection.
[23]	Delamination thickness estimation	IDFT-based time domain reflectometry Microwave NDT	**High**: The technique was able to estimate the thickness of shallow delamination with relatively narrow bandwidth	**High**: The estimation technique is based on the oversampling the time domain reflections by using N-points IDFT, which increases the complexity of the process to be $O(N^2)$ for each scanned location.
[This Work]	Delamination thickness estimation	IFFT-based Microwave NDT	**High**: The proposed technique is able to estimate delamination in dielectric of less than 1 mm using an OERW probe of 13.5 GHz bandwidth	**Low**: The conversion to the time domain is achieved using the IFFT algorithm ($O(N\ logN)$ for each scanned location), and the remaining signal processing steps do not add much to the complexity of the NDT approach.

techniques seems to be unable to correctly identify delamination locations with thickness below 0.2 *mm*.

Given the relatively narrow bandwidth used for these measurements, detecting and estimating the thickness of sub-millimeter thick delamination without excessive post-processing steps is significantly promising. When compared to other NDT technique, the proposed approach is able to achieve the required material evaluation without increasing the complexity and the cost of the setup (as in the IRT technique), not to mention maintaining the speed of the NDT process to achieve real-time applicability. This technique is also advantageous over the THz NDT technology since it is based on the same principle but using much simpler apparatus, smaller bandwidth, and low-complexity post-processing steps. As for other microwave-related NDT techniques, the proposed approach provides better results while reducing the processing time by using the efficient IFFT algorithm to obtain the time domain reflection coefficient. Compared to an $N-$points IDFT with the computational complexity per scanned location given by $O(N^2)$, the IFFT algorithm reduces

the complexity for the same processes to $O(N\ logN)$ [34], which represents a significant advantage, especially for high values of N.

Table (1) illustrates most of the previously-reported similar microwave NDT approaches and their accuracy in estimating dielectric thickness as well as their relative computational complexities. When compared to these approaches, the technique proposed in this paper can be regarded as a promising candidate for quick and accurate identification of shallow delamination in dielectric coatings.

V. CONCLUSION

In this paper, a novel microwave NDT technique is proposed for detection and thickness estimation of delaminated regions in dielectric coatings. The technique is based on scanning the surface of the dielectric using an Open Ended Rectangular Waveguide (OERW) connected to a Vector Network Analyzer (VNA) that measures the reflection coefficient at specific frequency points within a pre-defined bandwidth. After processing the reflections from a reference location on the sample, the measured reflection coefficients for the rest of the sample are converted to the time domain using the Inverse Fast Fourier Transform (IFFT) algorithm. During the scan, the amplitude of the reflection coefficient at a certain time step is recorded, normalized, and converted to a dielectric thickness estimation. This technique has been validated by simulating a structure with OERW placed over a dielectric layer backed by metal and contains an air gap with varying thickness to account for a delamination. The results show that the proposed technique is able to estimate the thickness of the delmaination to a high degree of accuracy. Moreover, Two samples with different machined delamination regions have been tested and analyzed. The results show that the proposed technique succeeds in detecting delamination of thickness down to 0.2 mm, with correct estimation for delamination thickness from 0.4 mm to 1.5 mm. The outcomes of the simulation and measurement tests prove the validity of the proposed technique as a promising approach for accurate delamination detection in the real-time.

REFERENCES

[1] R. A. Miller, "Thermal barrier coatings for aircraft engines: History and directions," *J. Thermal Spray Technol.*, vol. 6, no. 1, p. 35, 1997.

[2] T. Fukuchi, T. Ozeki, M. Okada, and T. Fujii, "Nondestructive inspection of thermal barrier coating of gas turbine high temperature components," *IEEJ Trans. Elect. Electron. Eng.*, vol. 11, no. 4, pp. 391–400, 2016.

[3] J. I. Eldridge, C. M. Spuckler, and R. E. Martin, "Monitoring delamination progression in thermal barrier coatings by mid-infrared reflectance imaging," *Int. J. Appl. Ceram. Technol.*, vol. 3, no. 2, pp. 94–104, Mar. 2006.

[4] P. J. Shull, *Nondestructive Evaluation: Theory, Techniques, and Applications*. Boca Raton, FL, USA: CRC Press, 2002.

[5] P. F. Gobin, Y. Jayet, J. C. Baboux, M. Salvia, A. Chateauminois, J. C. Abry, and G. Giraud, "New trends in non-destructive evaluation in relation to the smart materials concept," *Int. J. Syst. Sci.*, vol. 31, no. 11, pp. 1351–1359, Jan. 2000.

[6] L. Cheng and G. Y. Tian, "Comparison of nondestructive testing methods on detection of delaminations in composites," *J. Sensors*, vol. 2012, Apr. 2012, Art. no. 408437.

[7] N. H. Hadi and B. J. Hamood, "Vibration analysis of a composite plate with delamination," *J. Eng.*, vol. 21, no. 2, pp. 144–164, 2015.

[8] G. Chen, "Non-destructive evaluation (NDE) of the failure of thermal barrier coatings," in *Thermal Barrier Coatings*. Amsterdam, The Netherlands: Elsevier, 2011, pp. 243–262.

[9] F. Yu and T. D. Bennett, "Phase of thermal emission spectroscopy for properties measurements of delaminating thermal barrier coatings," *J. Appl. Phys.*, vol. 98, no. 10, Nov. 2005, Art. no. 103501.

[10] V. P. Vavilov, S. Marinetti, F. Cernuschi, and D. Roba, "Thermal nondestructive testing of thermal-barrier coatings of turbine buckets," *Russian J. Nondestruct. Test.*, vol. 41, no. 7, pp. 466–472, 2005.

[11] R. Shrestha and W. Kim, "Evaluation of coating thickness by thermal wave imaging: A comparative study of pulsed and lock-in infrared thermography—Part I: Simulation," *Infr. Phys. Technol.*, vol. 83, pp. 124–131, Jun. 2017.

[12] Y. Liu, G. Zhao, Y. Du, and Y. Zhang, "Thermal barrier coating debonding defects detection based on infrared thermal wave testing technology under linear frequency modulation heat exitation," *Thermal Sci.*, vol. 23, no. 3, pp. 1607–1613, 2019.

[13] W. Zhu, Z. Liu, D. Jiao, and H. Xie, "Eddy current thermography with adaptive carrier algorithm for non-destructive testing of debonding defects in thermal barrier coatings," *J. Nondestruct. Eval.*, vol. 37, no. 2, pp. 1–12, Jun. 2018.

[14] D.-C. Jiao, Z.-W. Liu, W.-Y. Zhu, and H.-M. Xie, "Exact localization of debonding defects in thermal barrier coatings," *AIAA J.*, vol. 56, no. 9, pp. 3691–3700, Sep. 2018.

[15] F. Wang, J. Liu, O. Mohummad, and Y. Wang, "Research on debonding defects in thermal barrier coatings structure by thermal-wave radar imaging (TWRI)," *Int. J. Thermophys.*, vol. 39, no. 6, p. 71, 2018.

[16] D. Ye, W. Wang, J. Huang, X. Lu, and H. Zhou, "Nondestructive interface morphology characterization of thermal barrier coatings using terahertz time-domain spectroscopy," *Coatings*, vol. 9, no. 2, p. 89, Feb. 2019.

[17] S. Unnikrishnakurup, J. Dash, S. Ray, B. Pesala, and K. Balasubramaniam, "Nondestructive evaluation of thermal barrier coating thickness degradation using pulsed IR thermography and THz-TDS measurements: A comparative study," *NDT E Int.*, vol. 116, Dec. 2020, Art. no. 102367.

[18] M. Sayar, D. Seo, and K. Ogawa, "Non-destructive microwave detection of layer thickness in degraded thermal barrier coatings using K-and W-band frequency range," *NDT & E Int.*, vol. 42, no. 5, pp. 398–403, 2009.

[19] S. Guorong, Y. Tianting, H. Cunfu, Y. Shen, L. Yan, and W. Bin, "Detection of surface crack on the substrate under thermal barrier coatings using microwave non-destructive evaluation," *J. Microw. Power Electromagn. Energy*, vol. 49, no. 2, pp. 69–75, 2015.

[20] M. F. AJK, R. Sloan, C. I. Duff, M. Wielgat, and J. F. Knowles, "Nondestructive testing of thermal barrier coated turbine blades using microwave techniques," *Mater. Eval.*, vol. 74, no. 4, pp. 543–551, 2016.

[21] M. F. Akbar, G. N. Jawad, L. R. Danoon, and R. Sloan, "Delamination detection in glass-fibre reinforced polymer (GFRP) using microwave time domain reflectometry," in *Proc. 15th Eur. Radar Conf. (EuRAD)*, Sep. 2018, pp. 253–256.

[22] R. Sutthaweekul, G. Tian, Z. Wang, and F. Ciampa, "Microwave open-ended waveguide for detection and characterisation of FBHs in coated GFRP pipes," *Compos. Struct.*, vol. 225, Oct. 2019, Art. no. 111080.

[23] M. F. Akbar, G. N. Jawad, L. D. Rashid, and R. Sloan, "Nondestructive evaluation of coatings delamination using microwave time domain reflectometry technique," *IEEE Access*, vol. 8, pp. 114833–114841, 2020.

[24] S. Bakhtiari, S. I. Ganchev, and R. Zoughi, "Open-ended rectangular waveguide for nondestructive thickness measurement and variation detection of lossy dielectric slabs backed by a conducting plate," *IEEE Trans. Instrum. Meas.*, vol. 42, no. 1, pp. 19–24, Feb. 1993.

[25] R. Zoughi, J. R. Gallion, and M. T. Ghasr, "Accurate microwave measurement of coating thickness on carbon composite substrates," *IEEE Trans. Instrum. Meas.*, vol. 65, no. 4, pp. 951–953, Apr. 2016.

[26] C. Reece, "Simple method for determining cable length resistance in time domain reflectometry systems," *Soil Sci. Soc. Amer. J.*, vol. 62, no. 2, pp. 314–317, 1998.

[27] M. F. Akbar, G. N. Jawad, and L. D. Rashid, "Delamination thickness estimation using microwave time domain reflectometry," in *Proc. 16th Eur. Radar Conf. (EuRAD)*, 2019, pp. 147–194.

[28] R. Ludwig, *RF Circuit Design: Theory & Applications*, 2nd ed London, U.K.: Pearson, 2000.

[29] P. Stenius and B. York, "On the propagation of transients in waveguides," *IEEE Antennas Propag. Mag.*, vol. 37, no. 2, pp. 39–44, Apr. 1995.

[30] R. Collin, *Field Theory Guided Waves* (The Institute of Electrical and Electronics Engineering), 2nd ed. New York, NY, USA: IEEE Press, 1991.

[31] G. A. Ybarra, S. M. Wu, G. L. Bilbro, S. H. Ardalan, C. P. Hearn, and R. T. Neece, "Optimal signal processing of frequency-stepped CW radar data," *IEEE Trans. Microw. Theory Techn.*, vol. 43, no. 1, pp. 94–105, Jan. 1995.
[32] (Jan. 2021). *FieldFox Handheld Analyzer*. Keysight Technologies. [Online]. Available: https://www.keysight.com/zz/en/assets/7018-03314/data-sheets/5990-9783.pdf
[33] (Apr. 2018). *Optimizing VNA Measurement Speed*. Accessed: May 29, 2021. [Online]. Available: https://coppermountaintech.com/optimizing-vna-measurement-speed/
[34] M. Heideman, D. Johnson, and C. Burrus, "Gauss and the history of the fast Fourier transform," *IEEE ASSP Mag.*, vol. 1, no. 4, pp. 14–21, Oct. 1984.
[35] M. T. Ghasr, M. J. Horst, M. Lechuga, R. Rapoza, C. J. Renoud, and R. Zoughi, "Accurate one-sided microwave thickness evaluation of lined-fiberglass composites," *IEEE Trans. Instrum. Meas.*, vol. 64, no. 10, pp. 2802–2812, Oct. 2015.
[36] B. Gao, H. Zhang, W. L. Woo, G. Y. Tian, L. Bai, and A. Yin, "Smooth nonnegative matrix factorization for defect detection using microwave nondestructive testing and evaluation," *IEEE Trans. Instrum. Meas.*, vol. 63, no. 4, pp. 923–934, Apr. 2014.
[37] N. H. M. M. Shrifan, M. F. Akbar, and N. A. Mat Isa, "Maximal overlap discrete wavelet-packet transform aided microwave nondestructive testing," *NDT E Int.*, vol. 119, Apr. 2021, Art. no. 102414.
[38] J. Hu, Y. Lia, J. Tana, W. Lia, and Z. Chen, "Characterization and imaging of localized thickness loss in GFRP with Ka-band microwave open-ended waveguides," in *Electromagnetic Non-Destructive Evaluation (XXIII)*, vol. 45. Amsterdam, The Netherlands: IOP Press, 2020, p. 218, doi: 10.3233/SAEM200036.
[39] M. S. U. Rahman, A. Haryono, Z. Akhter, and M. A. Abou-Khousa, "On the inspection of glass reinforced epoxy pipes using microwave NDT," in *Proc. IEEE Int. Instrum. Meas. Technol. Conf. (I2MTC)*, May 2019, pp. 1–5.
[40] Y. Xie, X. Yang, J. Yuan, and Z. Zhu, "Non-destructive evaluation of pipes by microwave techniques and artificial neural networks," *Meas. Sci. Technol.*, vol. 31, no. 12, Dec. 2020, Art. no. 125402.
[41] N. H. M. M. Shrifan, G. N. Jawad, N. A. M. Isa, and M. F. Akbar, "Microwave nondestructive testing for defect detection in composites based on K-means clustering algorithm," *IEEE Access*, vol. 9, pp. 4820–4828, 2021.

GHASSAN NIHAD JAWAD (Member, IEEE) was born in Baghdad, Iraq, in 1984. He received the B.Sc. and M.Sc. degrees in electronics and communication engineering from the University of Baghdad, Baghdad, in 2005 and 2009, respectively, and the Ph.D. degree from The University of Manchester, in 2016. He is currently a Lecturer with the University of Baghdad. His current research interests include microwave and millimeter-wave passive components, gyrotropic microwave devices, microwave nondestructive testing techniques, and short-range radar systems.

MUHAMMAD FIRDAUS AKBAR (Member, IEEE) received the B.Sc. degree in communication engineering from International Islamic University Malaysia (IIUM), Malaysia, in 2010, and the M.Sc. and Ph.D. degrees from The University of Manchester, Manchester, U.K., in 2012 and 2018, respectively. From 2010 to 2011, he was a Research and Development Engineer with Motorola Solutions, Penang, Malaysia. From 2012 to 2014, he was an Electrical Engineer with Usains Infotech Sdn Bhd, Penang. He is currently a Senior Lecturer with Universiti Sains Malaysia (USM). He is the Founder and the Director of Visionlytics Sdn Bhd. His current research interests include electromagnetics, microwave non-destructive testing, and microwave sensor and imaging.